UNIVERSAL WISER
PUBLISHER

Research Article

Synthesis of O3-$Na_{0.8}Fe_{0.6}Mn_{0.3}O_2$ Positive Electrode and Its Application to Sodium Ion Batteries

M. Alam Khan [ID]

Department of Energy and Materials Engineering, Dongguk University-Seoul, Seoul, Republic of Korea
E-mail: alamkhan77@gmail.com

Abstract: Herein, we report precise variation of Fe and Mn constituent in the sodium magnate layered cathodes with the compositions of $Na_{0.8}Fe_{0.4}Mn_{0.5}O_2$, $Na_{0.8}Fe_{0.5}Mn_{0.4}O_2$, $Na_{0.8}Fe_{0.6}Mn_{0.3}O_2$, $Na_{0.8}Fe_{0.6}Mn_{0.4}O_2$, $Na_{0.8}Fe_{0.7}Mn_{0.4}O_2$, $Na_{0.9}Fe_{0.6}Mn_{0.3}O_2$ in order to attain a high performing cathode. Based on this transition metal stoichiometry, an interesting sodium magnate combination of $Na_{0.8}Fe_{0.6}Mn_{0.3}O_2$, with O3-type crystal phase, possess R3m space group along with the superior electrochemical behavior is obtained. On charge-discharge capacities in the range of 2.0-3.8 V at 0.1 C, it shows the comparatively higher performance of the first and the second charge capacity of 115 and 180 mAhg^{-1} and discharge capacity of 184 and 181 mAhg^{-1}, respectively. The best sample was then compared with the closely related $Na_{0.8}Fe_{0.6}Mn_{0.4}O_2$, $Na_{0.9}Fe_{0.6}Mn_{0.3}O_2$ combination in terms of valence ratio and influence of excess sodium for the structure robustness, stability along with purity. The best sample with the composition $Na_{0.8}Fe_{0.6}Mn_{0.3}O_2$ does not show detectable impure phase while $Na_{0.8}Fe_{0.6}Mn_{0.4}O_2$ and $Na_{0.9}Fe_{0.6}Mn_{0.3}O_2$ shows a tendency of P-type (Cmca space group) behavior with 30.8% and 32.8%, respectively. The enhancement of iron constituent increases not only the performances but also the stabilization of sodium vacancy ordering and substitution of Mn with a substantial reduction of Jahn-Teller distortion, mounting biphasic characteristics and high peak intensity of 41.5 °.

Keywords: sodium magnate, O3-type cathode, layered structure, sodium-ion batteries, solid-state reaction

1. Introduction

Ever growing exigencies for a low-cost environment-friendly storage system with a sheer growing world population must be achieved by renewable means for sustainable future. Among the several potential options, Lithium-Ion Batteries (LIBs) are the most popular choice after their commercialization in 1991 by Sony. However, the lack of lithium availability and its unstable geographical distribution culminated in a massive rising in materials costs over the recent years [1] and it remains a pivotal barrier towards the splendid scalable energy storage battery system. Additionally, vis-a-vis to long-lasting ''stock'' target of 1 billion 40 kWh Li-based automobile batteries is close to the limit of what the current stock is available. Thus, there persists a paramount longing to turn up towards alternate choices, especially in view of state strategies to cultivate massive-scale energy storage grids and equipment for cheaper prices [2-5]. Thus, the extension of secondary battery research into alternative elements may stimulate the competence of scaling and cost challenges intrinsic to long-standing plans and it is imperative to seek inexpensive candidates which are not source-constricted [6]. Among many potential alternative choices, the layered oxides ($NaMO_2$, M = Mn, Fe, Co,

Ni, V, Cr) extend many edges owing to their simple structures, high capacities, superior stabilities and ease of synthesis.

Sodium as the world's 4th most abundant element has the potential to fulfill the economic and environmental issues in energy storage systems due to high abundance and ultra-low cost [7], second in size (1.02 Å), second in reducing capability (-2.71V vs. SHE (Li) = -3.04 V) and second lightest in alkaline earth metal family after lithium (0.76 Å), is an ideal alternative in secondary battery technology [8]. Although the research on sodium-ion batteries was started in the 1980s [9, 10] in parallel to the lithium-ion batteries but completely overshadowed by the superior electrochemical properties of the LIBs [11]. Lately, there is a surge of research publication based on sodium systems as promising electrode materials [12-14] with different synthetic conditions (temperature, concentration and slow/fast cooling) in solid-state chemistry. Among various promising alternatives, the sodium magnate layered oxides possessing P2 or O3 structures forming $(MO_2)n$ sheets, between which the sodium cation is coordinated to octahedral (O), or prismatic (P) sites where transition metal layers repeating in a unit cell ABCABC in O3, ABBA in P2 are highly appealing [15].

Initially, a single transition metal layered oxides ($NaMO_2$) was reported [16] where multiple advantages were noticed such as radius of Na^+ ion much larger than transition metal ion preventing cation mixing (that is severe in Li^+ ion oxide batteries), the inactive redox couples vs. Li can be used in sodium cells as $Cr^{3+/4+}$ and the tolerance of higher vacancy concentrations of sodium can be exploited well [17]. However, strong Na^+/vacancy interactions may result in multiple structural transitions upon cycling, considerably affecting the electrode ageing properties [16]. To avoid this bottleneck, two approaches are employed; one is to limit the cutoff voltages to 3.8 V [18] and the other is the cation stabilization by bi-phasic reaction following the report of Yabuuchi et al. ($P2-Na_xFe_{0.5}Mn_{0.5}O_2$) [17], where many plateaus as observed in case of Na_xMnO_2 were eliminated in their charge-discharge curves. Afterwards, Mn and Fe-based electrode materials were seen as potential candidates owing to the elemental abundance, low cost and promising electrochemical performances. It has been reported that intermixing of various transition metals (Ni, Co, Mn, Fe, Ti) in the MO_2 sheets improves the structural stability and electrochemical performances in sodium-ion batteries [19, 20]. However, this phenomenon was not found in all cases and it has been documented that the potentiostatic charge-discharge curve of O3-phase containing $NaNi_{0.5}Mn_{0.5}O_2$ exhibits multiple plateau behavior [21] despite bimetallic while P2-phase $Na_xNi_{1/3}Mn_{2/3}O_2$ shows a smooth charge-discharge curve [22]. In the comparative performance of P2-phase $Na_{2/3}Fe_{1/2}Mn_{1/2}O_2$ and O3-phase $NaFe_{1/2}Mn_{1/2}O_2$, it has been found that the P2-phase manifests superb electrochemical ability by dispensing a reversible capacity of 190 mAhg[-1] within the voltage range of 1.5-4.2 V at a current density of 12 mAhg[-1] while O3-phase delivered lower with 100-110 mAhg[-1] of reversible capacity under similar conditions even though the capacity retention rate is almost resembling. Since in the $Na_xFe_xMn_{1-x}O_2$ ($1.0 \leq x \leq 0.5$) layered cathodes, when the x > 0.65, the O3-phase is dominantly stabilized while x < 0.65, a combination of two or more O3- and P2-like phases is composed [23]. Additionally, the capacity, reversibility, capacity retention and polarization are enriched as the Mn concentration beefed up to x = 0.5. But the Mn is highly Jahn-Teller active and the ensuing distortions could be addressed by less active Jahn-Teller ions for the composite metal ions and it's been reported that the addition of $Fe^{3+/4+}$ high redox constituent, the capacity recede became less pronounced [24, 25]. Indeed, sodium content ($Na_{2/3}$) has been achieved as a benchmark for the layered oxide electrode preparation in general, however, it's also important to elucidate meticulous details of optimum doses of Na along with transition metals in the O3 phase for the suitable, efficient and recyclable electrochemical performances as the amount of sodium influences electrochemical performances. The intrinsic properties of cathodes are also largely dependent on the transition metal contents, and there would be a trade-o relationship of thermal stability and cycling stability characteristics [26]. Herein, we report excellent cathode material with a composition of $Na_{0.8}Fe_{0.6}Mn_{0.3}O_2$ with a slight increment of Na along with the transition metal ratio variation (Fe, Mn) in search of an efficient positive electrode in respect to electrochemical performance and structure stability by using the solid-state reaction method at 700 °C under fast cooling, as we have reported previously for sodium magnate [27]. The influences of other compositions were also analyzed where a slight difference in transition metal constituent substantially affects the performance capabilities in sodium-ion battery application.

2. Experimental section

Sample Synthesis: The samples containing various amounts of sodium, iron and manganese ($NaFeMnO_2$) metals with the O3-phase were synthesized by a solid-state reaction method with a stoichiometric amount of Na_2CO_3

(Aldrich), Fe_2O_3 (Aldrich) and Mn_2O_3 (Aldrich) at 700 °C for 10 h in the continuous airflow of 1 ml/cm^3 in the tube furnace (Daesung Co., Ltd). The ratios of Na:Fe:Mn were maintained as 0.8:0.6:0.3 in the best sample and other ratios (0.7:0.5:0.5, 0.8:0.4:0:5, 0.8:0.5:0.4, 0.8:0.3:0.6, 0.8:0.6:0.4, 0.8:0.7:0.4, 0.9:0.6:0.3) were maintained and first ball milled (FRITSCH, Pulverisette) in acetone as solvent at 300 rpm/min for the 3 h, then dried and made as thin pellets using 0.4 g sample pressed manually. The obtained samples were then placed in a tube furnace and after reaction immediately taken and placed in the glove box. The pellets were powdered by using mortar before the slurry fabrication for electrochemical and characterization study and kept respectively in argon-filled glove box in the sealed vials.

Characterizations of prepared samples: The crystal structures of the synthesized $NaFeMnO_2$ samples were characterized by powder X-ray diffraction (Rigaku XRD-6000 Cu-Kα radiation, l51.5418 Å). The diffraction data were scanned at the rate of 2 °/min in the 2θ range of 10-70 °. The nanoparticle morphology details were analyzed by a field emission scanning electron microscope (FE-SEM) (S-4300 Shimadzu, 15 kV). The Cyclic Voltammetry (CV) was also applied with a scan rate of 0.1 mV between 2.0 and 3.8 V vs. Na/Na$^+$ by the Wonatech WBCS 3000 system (Korea). X-ray Absorption Near-Edge Structure (XANES) spectra data was recorded by Beamline 7 D and 8 C at the PAL, Republic of Korea.

Electrochemical analysis: The electrochemical performance studies of cycling tests were performed by fabricating coin cells (CR-2032) in the glove box. First, the electrode slurries were prepared by a mixture of active materials ($NaFeMnO_2$) with various compositions with acetylene black and Polyvinylidene Fluoride (PVDF) in the weight ratio of 80:10:10 with some additional drops of N-methyl-2-pyrrolidone (NMP), then pasted by doctor blade on the aluminum foil which was dried at 120 °C for 5 h in the vacuumed oven before the cell assembling. A half-cell was assembled using the prepared electrode as a cathode, a piece of separator (Celgard 2500), pure Na ingots for foil as the cathode, and electrolyte (1 M $NaPF_6$ in EC: DEC organic solutions) were utilized. Similarly, all the samples were made separately from the same procedure for the sodium half cells. TOSCAT 3000U (Toyosystem Co., Ltd) battery tester was used to perform galvanic charge and discharge testing in which all of them were conducted in a voltage range of 2.0-3.8 V vs. Na/Na$^+$ (0.1 C) at ambient.

3. Results and discussion

The X-Ray Diffraction (XRD) analyses of as-synthesized samples with several closely analyzed compositions are presented in Figure 1 measured in the 2θ range of 10 °-70 °. They were prepared with varying Fe to Mn ratio content starting from the well-known layered cathode ($Na_{0.7}Fe_{0.5}Mn_{0.5}O_2$) [17] in order to attain superior performing cathodes in terms of metal content optimization, reduction in Jahn-Teller distortion, purity and stability of O3-crystal structures. From the X-ray diffraction it has been inferred as all the synthesized materials possess a dominant O3 crystal structure phase with the R3m space group, mostly matches with the referenced ICSD85825 and indexed as 2θ position of 15.8 °, 32.0 °, 35.2 °, 39.0 °, 41.5 °, 43.0 °, 48.9 °, 52.9 °, 62.6 °, 64.8 °, 67.0 ° corresponding to (003), (006), (101), (102), (104), (105), (009), (107), (110), (1010), (113) phases [28]. However, in addition to the above peaks at 2θ positions at 61 ° found only in $Na_{0.8}Fe_{0.4}Mn_{0.5}O_2$ sample while peaks at 61 ° and minor at 37 ° are observed in $Na_{0.8}Fe_{0.5}Mn_{0.4}O_2$ due to the high content of sodium ion in O3 structure owing to shrinkage of transition metal layer due to oxidation of Fe^{3+} and Co^{3+} as reported in in-situ XRD study [29]. The XRD patterns corresponding to the other peaks in $Na_{0.7}Fe_{0.5}Mn_{0.5}O_2$, $Na_{0.8}Fe_{0.4}Mn_{0.4}O_2$, $Na_{0.8}Fe_{0.5}Mn_{0.4}O_2$ in Figure 1 show almost similar tendency with a strong layered peak at 15.8 °. However, a very interesting XRD pattern is observed where the increase of Mn content ($Na_{0.8}Fe_{0.3}Mn_{0.6}O_2$) and a decrease in the position of the peak of 41.5 ° are observed but with the increase of Fe content ($Na_{0.8}Fe_{0.6}Mn_{0.3}O_2$), a sharp increase in this particular peak was noticed. Additionally, the crystallinity of all other peaks was sharper with the appearance of two new peaks at 37 ° and 68 ° owing to the oxidation of transition metals and shrinkage of O3 crystal due to excess of sodium [29]. The observed results could be inferred that Mn has a tendency to lower the crystallinity while Fe enhances this tendency that might give us clues about the better electron transport in iron-containing samples. The figure also shows XRD pattern of further variation in the transition metal content as $Na_{0.8}Fe_{0.6}Mn_{0.4}O_2$, $Na_{0.8}Fe_{0.7}Mn_{0.4}O_2$, and $Na_{0.9}Fe_{0.6}Mn_{0.3}O_2$ where good crystallinity with broad peaks but similar patterns were observed. Furthermore, in Supporting Information (SI) of Figure 1, presented XRD pattern by the slight increment of only Na content (Na_1 and $Na_{1.1}$) while keeping well-known ratio of $Na_{0.7}Fe_{0.5}Mn_{0.5}O_2$ as cathode where it is worthy to

note that when there is an increase of Na content ($Na_{1.1}$), a loss of crystallinity and structures was observed clearly that speculates us its crystal is destabilized in excess of Na content, consequently loss of performances and crystal structure deformation was inevitable as observed in the electrochemical test that can be seen in the supporting information of Figure 2. Nevertheless, it has been found that all the samples possess a dominant tendency mainly of O3-type crystal phase characteristics.
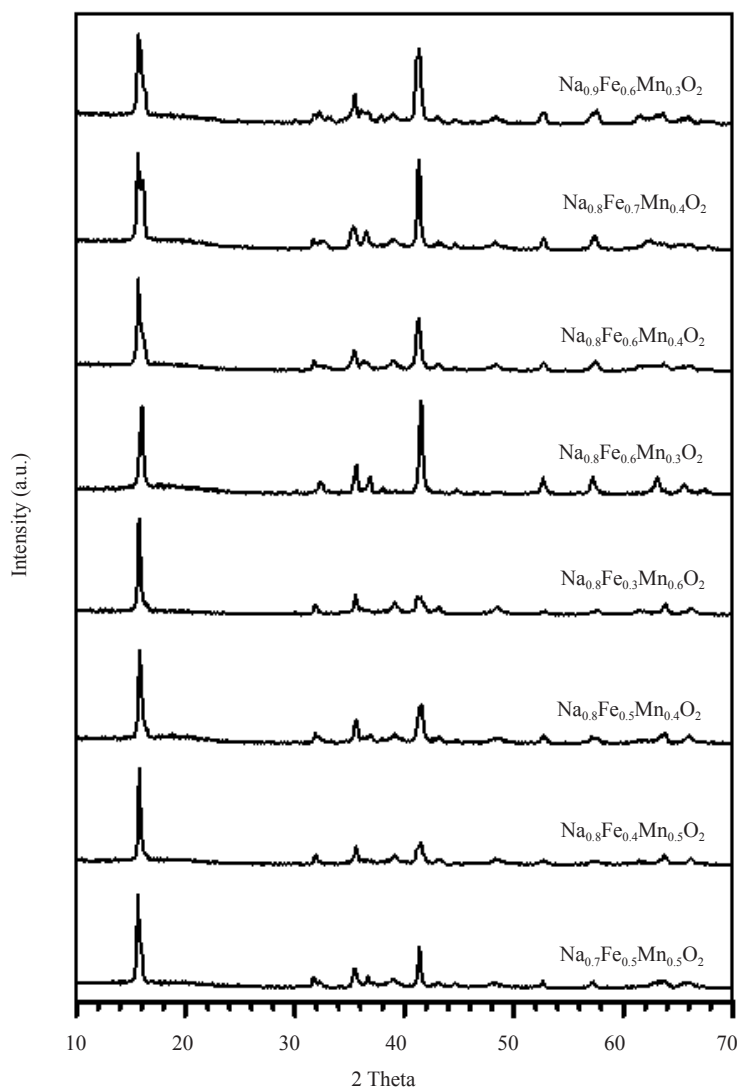
Figure 1. X-ray diffraction patterns of synthesized samples containing O-3 crystal structure with different Fe and Mn content as cathode materials

Figure 2(a) shows the galvanostatic performance of charge-discharge characteristics study with various amounts of Fe to Mn ratio analyzed at 2.0-3.8 voltage with a current density of 0.1 C, and each corresponding figure presenting stability variation with Coulombic efficiency data depicted in Figure 2(b). It can be observed that all the samples with different transition metal combinations show very different performances some delivering high and some low performances based solely on the metal content ratio combination, such results describe the high sensitivity towards the value of metal addition that even under the small content variation, possess similar XRD patterns, even with the same reaction synthesis condition, the crystal structure stability and performance were substantially affected. The best performance is obtained by the sample that contains $Na_{0.8}Fe_{0.6}Mn_{0.3}O_2$ combination where the first and second charge

capacities are 115 mAhg^{-1}, 180 mAhg^{-1} and the discharge capacities are 181 mAhg^{-1}, 184 mAhg^{-1}, respectively with capacity retention of 88%. However, the well-known and studied cathode $Na_{0.7}Fe_{0.5}Mn_{0.5}O_2$ in our case shows the first and second charge capacities as of 42 mAhg^{-1}, 100 mAhg^{-1}, and the discharge capacities are 101 mAhg^{-1} and 95 mAhg^{-1}, with capacity retention much lower than our best optimized Fe to Mn transition metals. In our quest for the efficient cathode search, when the metal combination switched to the $Na_{0.8}Fe_{0.5}Mn_{0.4}O_2$, worth fully we observed better the first and second charge capacities of 65 mAhg^{-1}, 125 mAhg^{-1} and the discharge capacities are 125 mAhg^{-1}, 121 mAhg^{-1} with a capacity retention of 90%, this result encourages us to explore more combinations in hope of better cathode material and on that note we tried several other variations systematically where we have speculated a trade-off of electrochemical performance, biphasic stability and reduced Jahn-Teller distortion might rectify [17], hence our best-obtained cathode is the ensuing results of $Na_{0.8}Fe_{0.6}Mn_{0.3}O_2$ following tedious experimental protocols. However, with $Na_{0.8}Fe_{0.4}Mn_{0.5}O_2$, $Na_{0.8}Fe_{0.3}Mn_{0.6}O_2$, $Na_{0.8}Fe_{0.6}Mn_{0.4}O_2$, $Na_{0.8}Fe_{0.7}Mn_{0.4}O_2$ and $Na_{0.9}Fe_{0.6}Mn_{0.3}O_2$ combinations, a lower in electrochemical performance of the first and second charge capacities of 35, 95 mAhg^{-1}, 35, 78 mAhg^{-1}, 40, 90 mAhg^{-1}, 70, 85 mAhg^{-1} and discharge the first and second capacities are 95, 90 mAhg^{-1} were observed, respectively. It's been observed from Figure 2, that electrochemical performances of cathode sample where the increase of Mn content $Na_{0.8}Fe_{0.3}Mn_{0.6}O_2$ carried out, a ladder-like curve appears similar to the sodium magnate cathode and similar to the single transition metal cathodes as we have reported [27], while increasing the Fe content, an increase in the first charge capacity and smooth curve was found. Probably sodium vacancy ordering is well stabilized by the slight substitution of Fe metal ions. In order to test the stability and longer retention time along with Coulombic efficiency, we have measured their characteristics and reported them in Figure 2(b). The results depicted a stable cyclic capacity up to 50 cycles in the best sample ($Na_{0.8}Fe_{0.6}Mn_{0.3}O_2$) having an average of 98.5% of Coulombic efficiency, the specific discharge capacities of the 2nd and 48th cycle 181.8 mAg^{-1} to 146 mAg^{-1} exhibiting capacity retention of 89.5%. It is worthy to note that the increase of Fe content electrochemical performance is improved until $Fe_{0.6}$ while the increase of Mn content performances decreases substantially and an optimum content $Fe_{0.6}Mn_{0.3}$ was observed in the best performing cathode in our study. Furthermore, in the case of the sample, where an enhance in sodium content was carried out to $Na_{0.9}$, still got a fairly good performance with no structural deformity as seen in XRD analysis, so we have carried out, an electrochemical analysis of other related samples with a combination of $Na_{0.8}Fe_{0.4}Mn_{0.5}O_2$, $Na_{0.8}Fe_{0.3}Mn_{0.6}O_2$, $Na_{0.8}Fe_{0.6}Mn_{0.4}O_2$, $Na_{0.8}Fe_{0.7}Mn_{0.4}O_2$, $Na_{0.9}Fe_{0.6}Mn_{0.3}O_2$ in order to understand the structural and electrochemical stability in detail. The structural stability of samples shows that with an increase of Mn content, the stability is much lower but with an increase of Fe, content stability is better, perhaps due to better stability and less Jahn-Teller distortion of crystal structures by the presence of Fe^{3+} ion which is low Jahn-Teller active metal. In order to ascertain the effect of higher voltage up to 2.0 to 4.2 V on the performance and stability, we have tested for the sample $Na_{0.8}Fe_{0.6}Mn_{0.3}O_2$, $Na_{0.8}Fe_{0.6}Mn_{0.4}O_2$, $Na_{0.9}Fe_{0.6}Mn_{0.3}O_2$ and the results are depicted in the figure of supporting information as Figure 3, where an obviously enhanced electrochemical performance was observed due to high voltages. However, no structural deformation was observed as well.

In order to get more insight, we choose three samples closely related for further characterization and structure studies to explore the change in local structures, phase transitions and sodium vacancy ordering responsible for voltage plateaus. Figure 3(a-c) shows the morphological feature of the as-synthesized $Na_{0.8}Fe_{0.6}Mn_{0.3}O_2$, $Na_{0.8}Fe_{0.6}Mn_{0.4}O_2$, $Na_{0.9}Fe_{0.6}Mn_{0.3}O_2$ nanocrystals analyzed by Field Emission Scanning Microscopy (FE-SEM). It has been observed that the smaller disc shape morphology possesses well-defined crystals typical to the layered structures [30] and most of the crystals found also agglomerated or fused each other by a topotactic effect of the solid-state reaction condition with the multidimension of the crystals are prominent forming a series of planes with an average size of ~500 nm in diameter where particles are clear with clear planes, but due to agglomeration, it's hard to clearly define the sizes. Although it is hard to get many clear differences between the samples by the FE-SEM micrographs, as visually observed more particle separation in the best sample was observed while in other sample particles were attached to the parent larger particles. Figure 3(d-f) depicts the Cyclic Voltammetry (CV) analysis of the corresponding samples in sodium half cells at a sweep rate of 0.1 mVs^{-1} in view to understand the electrochemical behavior for the first two cycles. The CV results depict typical peaks associated with electrochemical sodium (de)-intercalation process into the O3-layered structure, involving reversible processes in the 2-3.8 V potential region with a series of an anodic peak at 2.4 V (shoulder), (broad peak) 2.73 V, and 3.7 V while cathode peaks were 2.2 V, and 3.6 V, respectively. It has been reported that anodic/cathode peaks at 2.6/1.9 V are caused by Mn^{3+}/Mn^{4+} redox reactions and in our case, slight higher positions were found that ascribes

due to Fe substitution. The intensity of the peaks does not have many differences in successive cycles speculating low polarization, phase change, or irreversible structure variation on charging. Two dominant pairs of peaks are observed in both the anodic and cathode sweeps at 2.73 vs 2.2 V and 3.7 vs 3.6 V, corresponding to redox reactions of Mn^{3+}/Mn^{4+} and Fe^{3+}/Fe^{4+}, respectively [31, 32]. The higher anodic/cathode peak (1.73 V/2.2 V) may result from the higher Fe content and increased participation along with Mn^{3+}/Mn^{4+} redox couple in the overall as a complex electrochemical delithiation/lithiation process. Shoulders in the anodic peak at 2.06 V and 2.45 V are languishing in the second cycle which could be attributed to side reactions in the first cycle. The intensity of the peaks does not have much difference and overlapped well speculating of lower polarization, phase change or irreversible structure variation on charging successive cycles. The voltage plateaus associated with phase transitions are in good agreement with the corresponding charge-discharge curves in Figure 2. It is also interesting to point out that other samples (e, f) possess similar shapes of CV profiles compared to corresponding anodic/cathode reactions which may imply similar mechanisms of Na^+ transportation. However, the excess of Fe^{3+} effects on the performance is still not clear because of the complexity of the reaction at the current stage and detail study is going on. We ascribe that a larger quantity of Fe^{3+} constituent leads to a strong interaction between Mn-O bonds with stabilization of vacancy ordering by a partial excess amount of Fe substitution for Mn results in a biphasic reaction. It is considered that the intercalation and de-intercalation reaction of Na resulted in the occurrence of the peaks at voltages between 2.0 and 3.8 V.
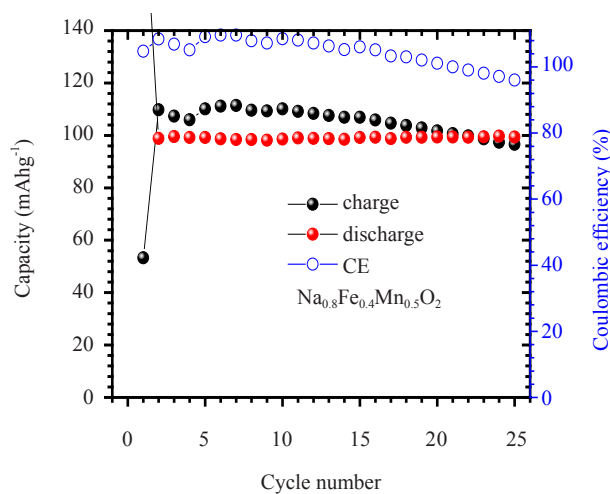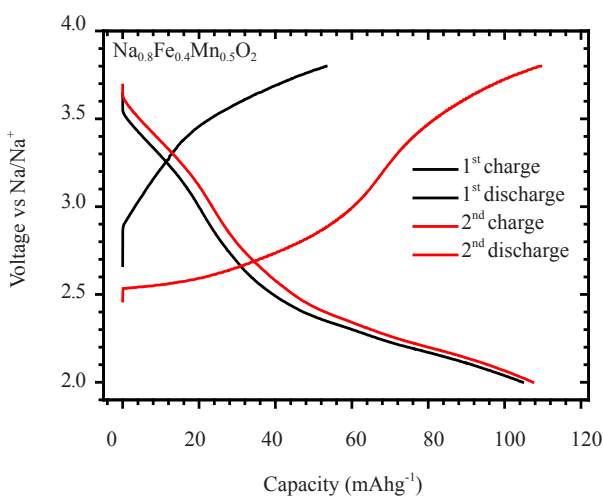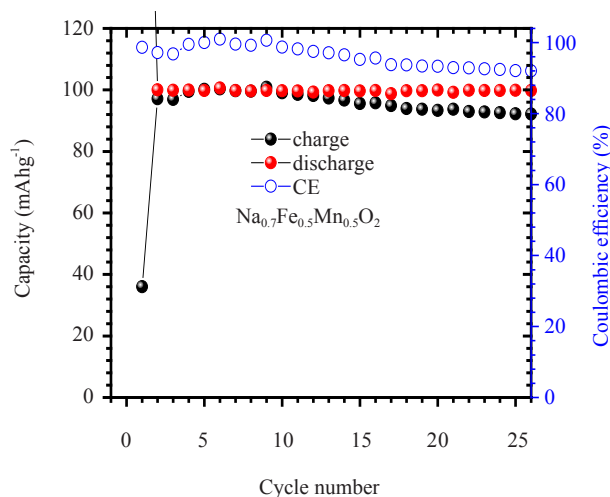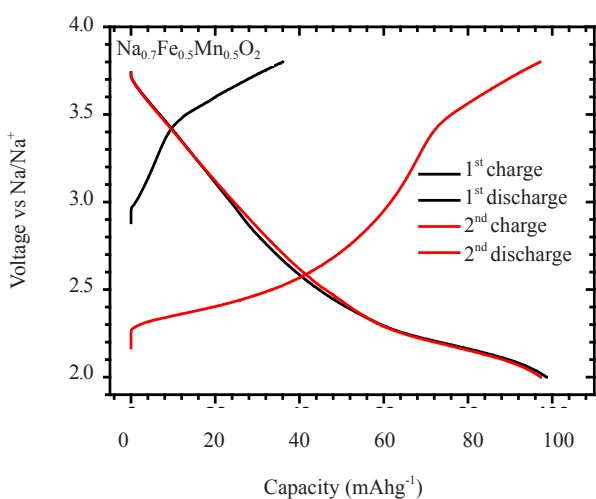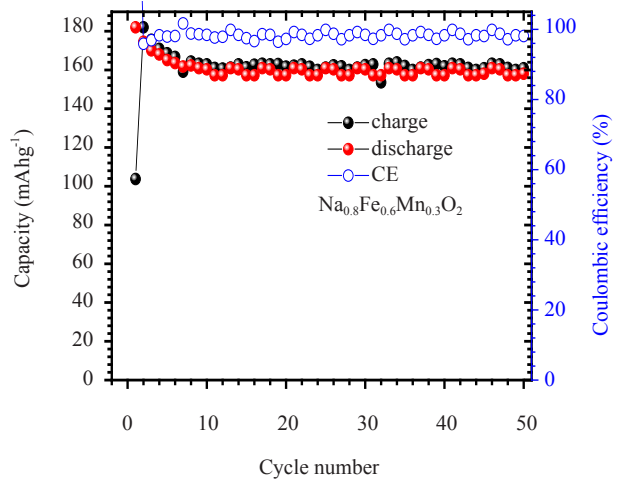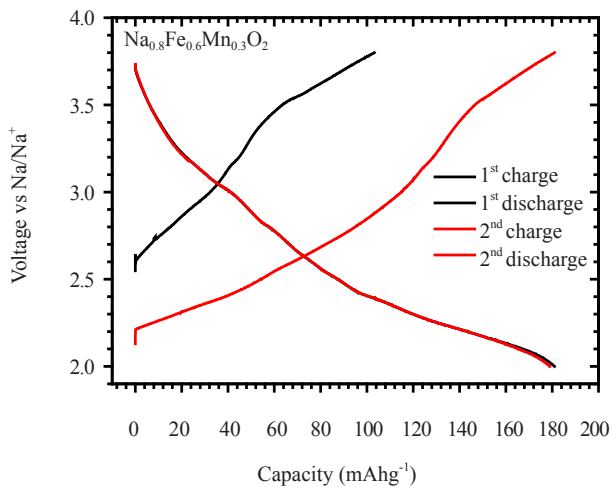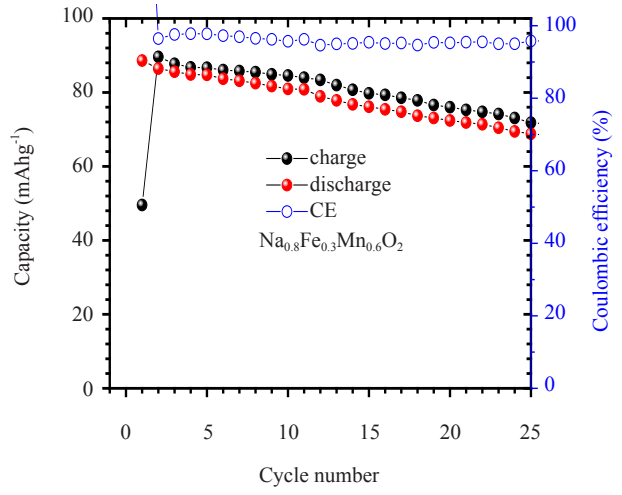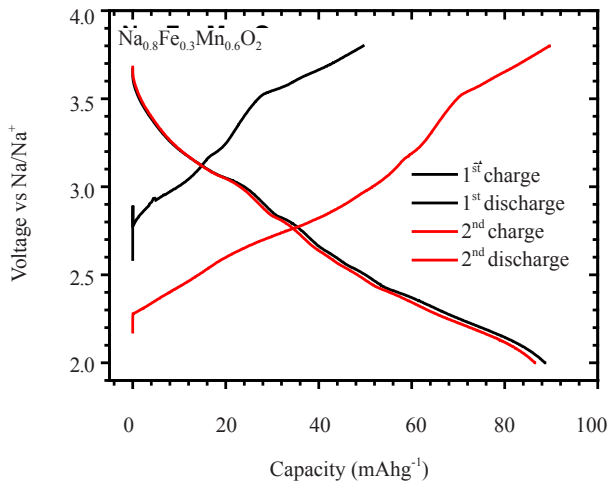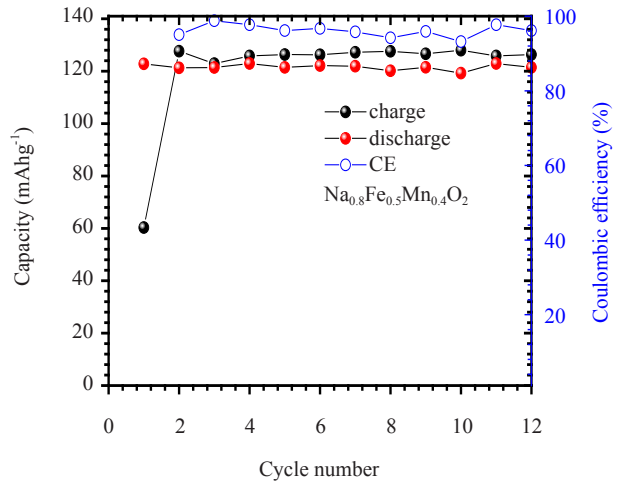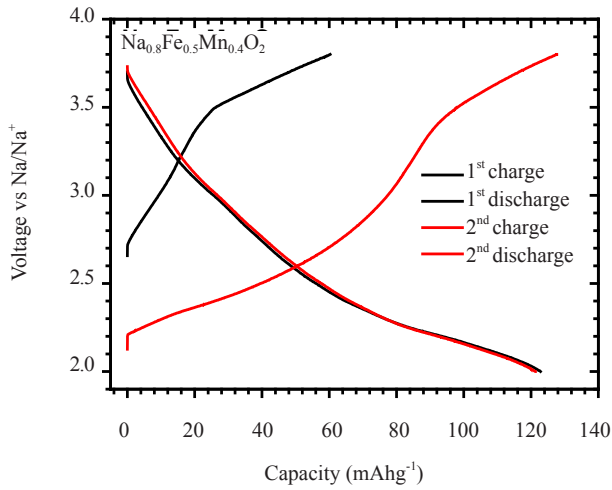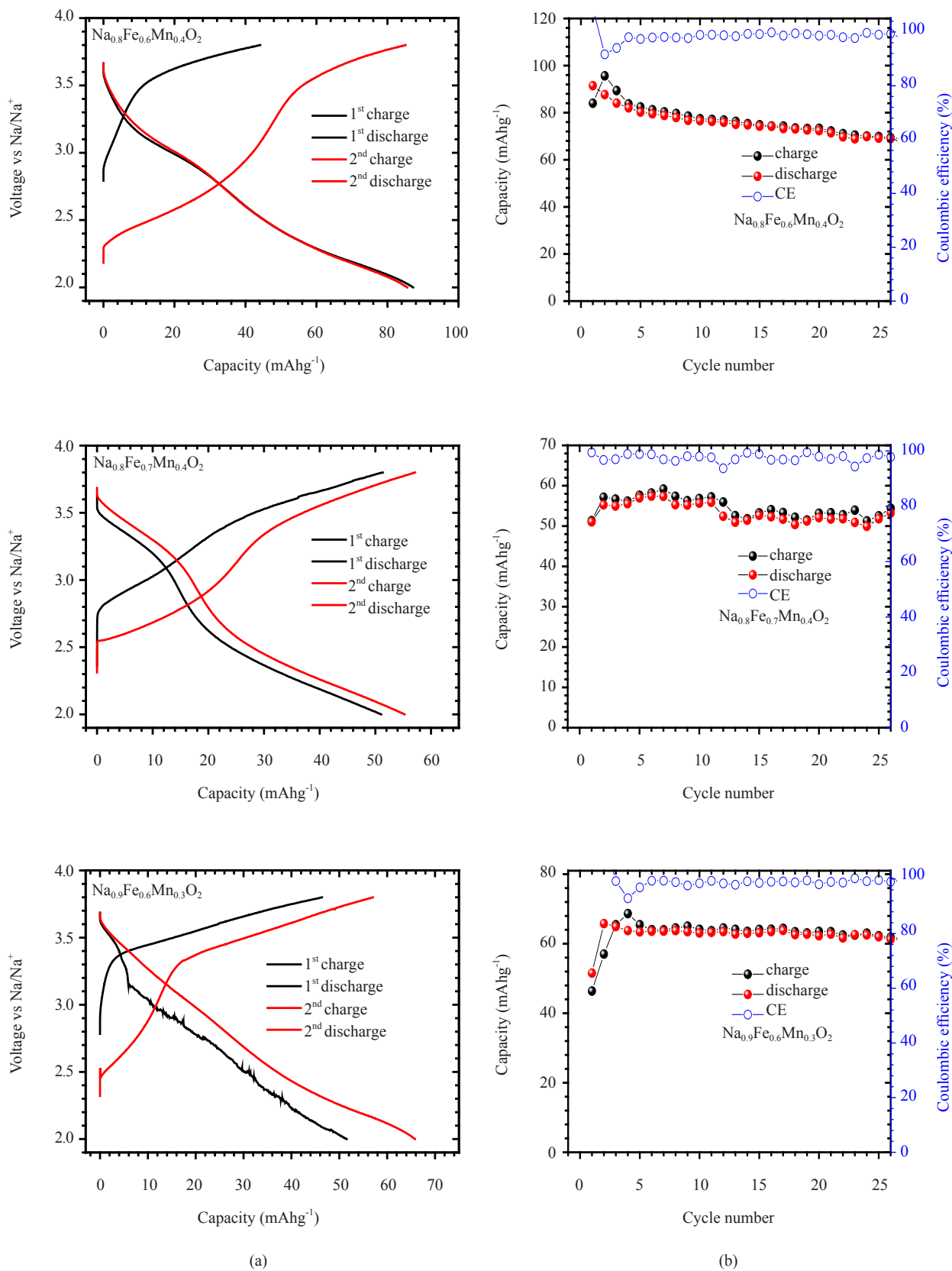
Figure 2. (a) Galvanostatic voltage profiles of synthesized samples containing O-3 crystal structure with different Fe and Mn content as cathode materials. (b) Corresponding cycle stability and Coulombic efficiency
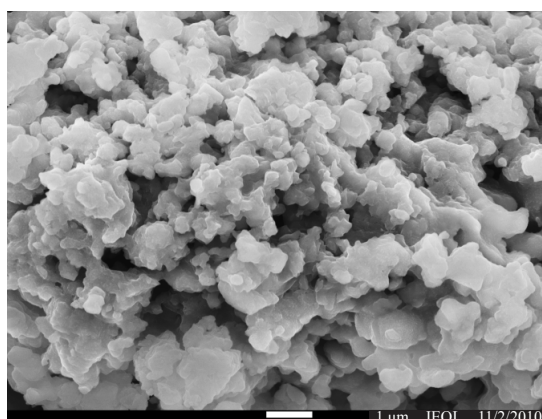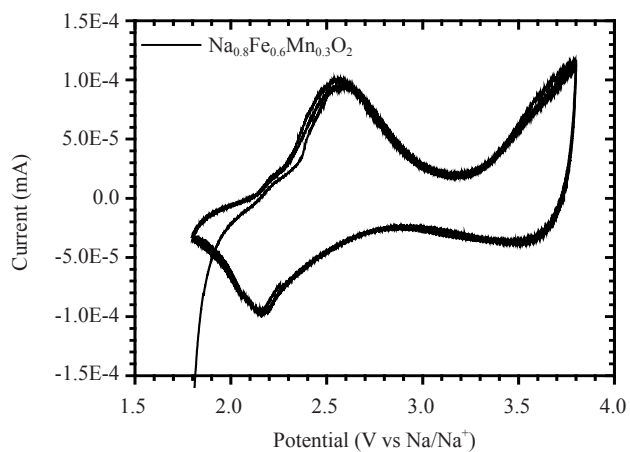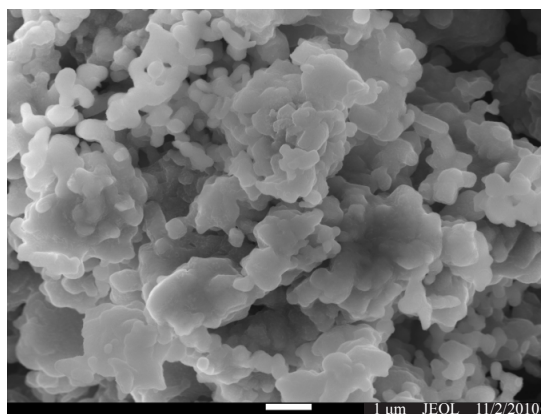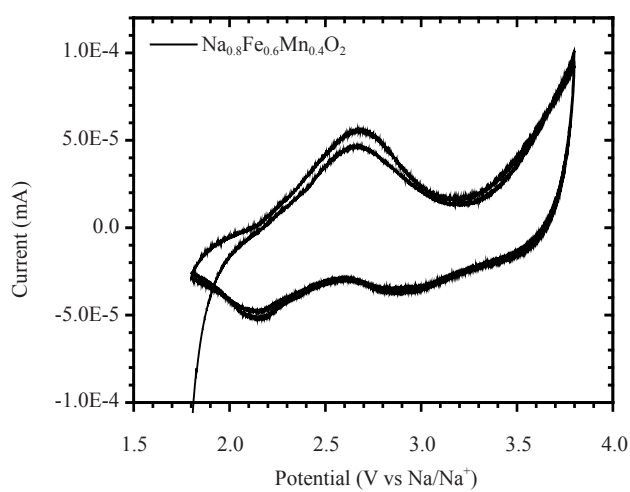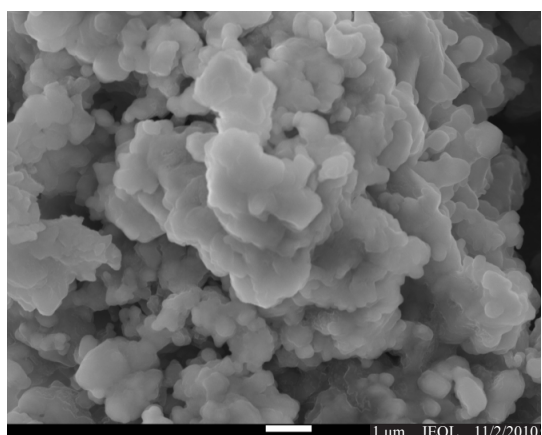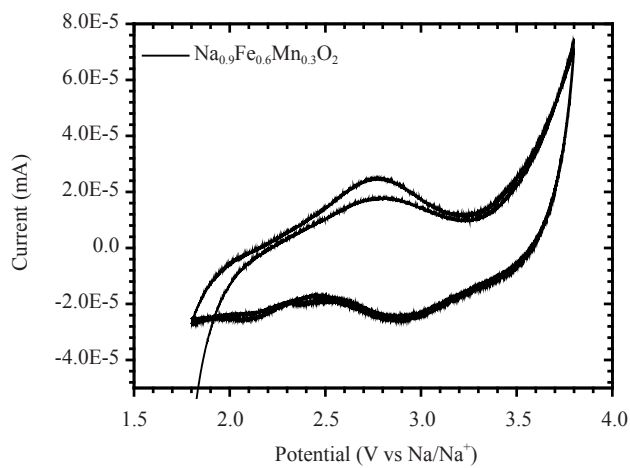
Figure 3. FE-SEM analysis of the synthesized samples (a-c) containing $Na_{0.8}Fe_{0.6}Mn_{0.3}O_2$, $Na_{0.8}Fe_{0.6}Mn_{0.4}O_2$, $Na_{0.9}Fe_{0.6}Mn_{0.3}O_2$ as cathode materials. (d-f) shows corresponding cyclic voltammograms of two selected cyclic sweeps
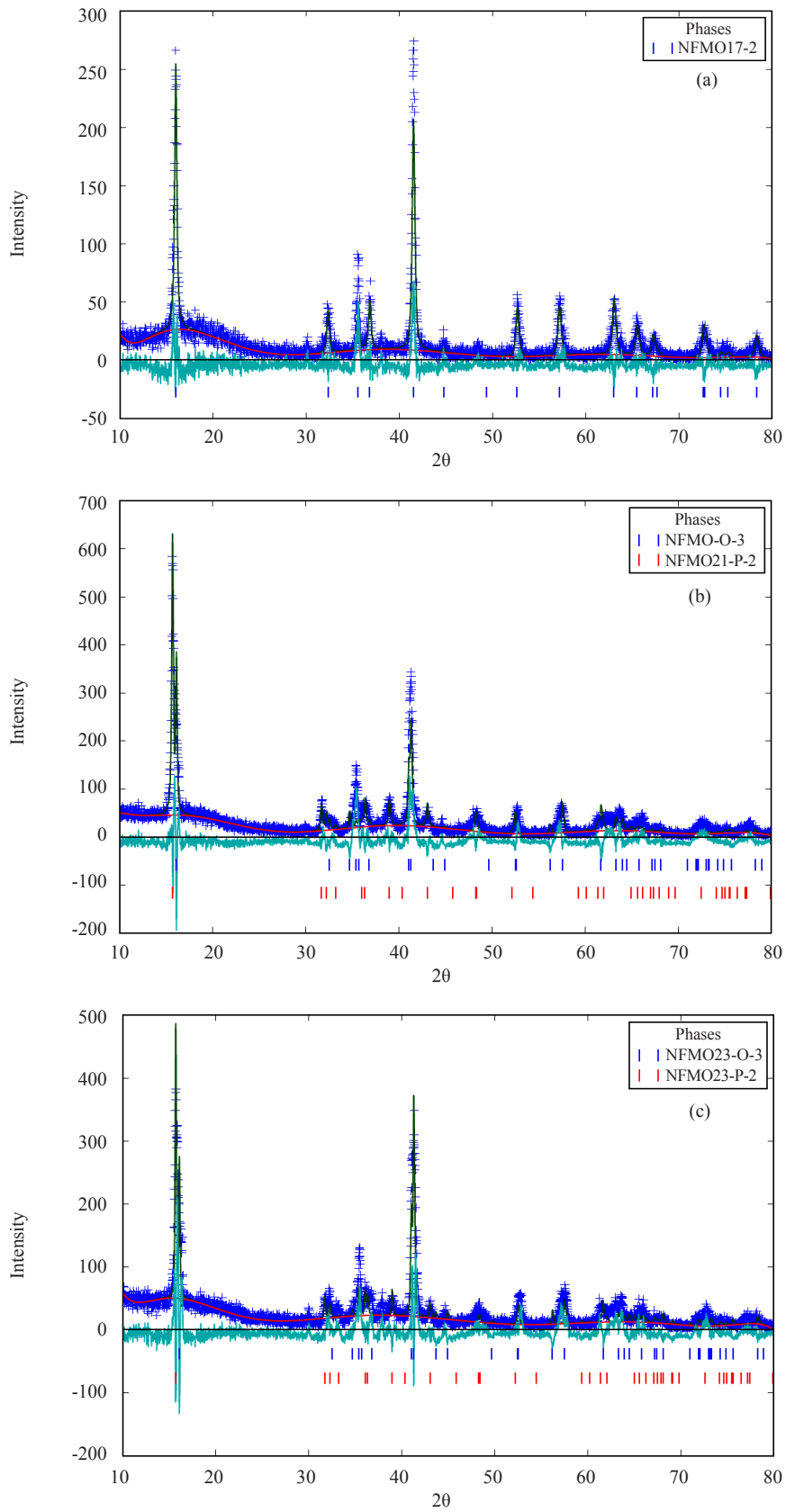
Figure 4. Rietveld refinement synthesized of samples (a-c) containing O-3 crystal structure with $Na_{0.8}Fe_{0.6}Mn_{0.3}O_2$, $Na_{0.8}Fe_{0.6}Mn_{0.4}O_2$, $Na_{0.9}Fe_{0.6}Mn_{0.3}O_2$ as cathode materials

The details of crystal peaks with a constituent composition of $Na_{0.8}Fe_{0.6}Mn_{0.3}O_2$ were analyzed by the Rietveld refinement and are presented in Figure 4(a), which gives the structural model of rhombohedral, Space Group (SG): R-3m with symmetry of a = 2.94667 (3) Å, b = 2.94667 Å, c = 16.59657 (2) Å with α = β = 90 ° and γ = 120 °, along with a satisfying convergence factor R_{wp} = 25.36. The significant larger c-parameter can be inferred as containing 3-layers with an interlayer spacing of 2.73 Å (VESTA software). No structural distortion eventuates which is due to the manifestation of high spin octahedral coordinated Fe^{3+} ($t^3 2g\ e^2 g$) and Mn^{4+} ($t^3 2g\ e^0 g$) where no Jahn-Teller induction is present. In our previous work, we have found more Mn^{4+} ion on the synthesis of O3 sample [27]. However, the Rietveld refinement of $Na_{0.8}Fe_{0.6}Mn_{0.4}O_2$, $Na_{0.9}Fe_{0.6}Mn_{0.3}O_2$ sample (Figure 4(b, c)) processes impurity peaks and some characteristics of P2 crystal phase with 30.8 and 32.8% as shown in Table 1 and 2. The Rietveld refinement showing a distortion with these P2-type structure with the Space group: *Cmca*: a = 2.84310 Å, b = 5.55644 Å, c = 11.28900 Å, α = β = γ = 90 ° with R_{wp} = 25.45, and *Cmca*: a = 2.84551 Å, b = 5.44682 Å, c = 11.27738 Å, α = β = γ = 90 ° with R_{wp} = 25.81, respectively. The minor variation among the values of the c_{hex} parameters could result from a minimal difference of Mn constituent between the samples. The *a* parameter for both phases is tantamount to each other since the oxide layers are constituted of analogous transition metals due to the fact that the number of layers in the unit cells are 3 layers for the O3-phase. In the O3 stacking, the interlayer distance is smaller because the oxygen atom of one layer (O1) displaced 1/3 of the unit cell with respect to the next oxygen (O2) in the adjacent oxygen layer, as a consequence of the variant space groups and interlayer spacing, some disparities can be detected in the XRD patterns. In our experimental protocol Fe^{3+}, Mn^{4+} and Mn^{3+} ions are anticipated to be present in materials containing an ample amount of non-Jahn-Teller Fe^{3+} and/or Mn^{4+} ions.

Table 1. Refined structural parameters of $Na_{0.8}Fe_{0.6}Mn_{0.3}O_2$ sample obtained from the Rietveld refinement using X-ray powder diffraction data at 297 K

$Na_{0.8}Fe_{0.6}Mn_{0.3}O_2$: Space group: *R3m*, $a_{hex.}$ = 2.944667Å, $c_{hex.}$ = 16.59657 Å, α = β = 90 °, γ = 120 °					
Atom	Wyckoff	Symmetry-a	Symmetry-b	Symmetry-c	Fraction
Na	3b	0.0000	0.0000	0.0000	0.800
Fe	3a	0.0000	0.0000	0.5000	0.600
Mn	3a	0.0000	0.0000	0.5000	0.300
O	6c	0.0000	0.0000	0.2250 (7)	1.000
Rwp = 25.23%					

Table 2. Refined structural parameters of $Na_{0.8}Fe_{0.6}Mn_{0.4}O_2$ sample obtained from the Rietveld refinement using X-ray powder diffraction data at 297 K

$Na_{0.8}Fe_{0.6}Mn_{0.4}O_2$: Space group: *R3m*, $a_{hex.}$ = 2.944667 Å, $c_{hex.}$ = 16.59657 Å, α = β = 90 °, γ = 120 °					
Atom	Multiplicity	Symmetry-a	Symmetry-b	Symmetry-c	Fraction
Na	2	0.0000	0.0000	0.5000	0.800
Fe	2	0.0000	0.5000	0.5000	0.600
Mn	2	0.0000	0.5000	0.5000	0.400
O	4	0.2030 (3)	0.0000	0.2031 (26)	1.000
Rwp = 28.13%					
$Na_{0.8}Fe_{0.6}Mn_{0.4}O_2$: Space group: *Cmca*, $a_{hex.}$ = 2.84310 Å, b = 5.556441, $c_{hex.}$ = 11.28900 Å, α = β = γ = 90 °					
Atom	Multiplicity	Symmetry-a	Symmetry-b	Symmetry-c	Fraction
Na1	16	-0.38631	0.33889	0.29800	0.109
Na2	16	-0.45926	0.71132	0.31527	0.231
Fe3	4	0.00000	0.00000	0.00000	0.400
Mn4	4	0.00000	0.00000	0.00000	0.600
O5	8	0.0000	0.70449	0.55222	1.000
Phase fraction: O3 = 69.2%, P2 = 30.8%					
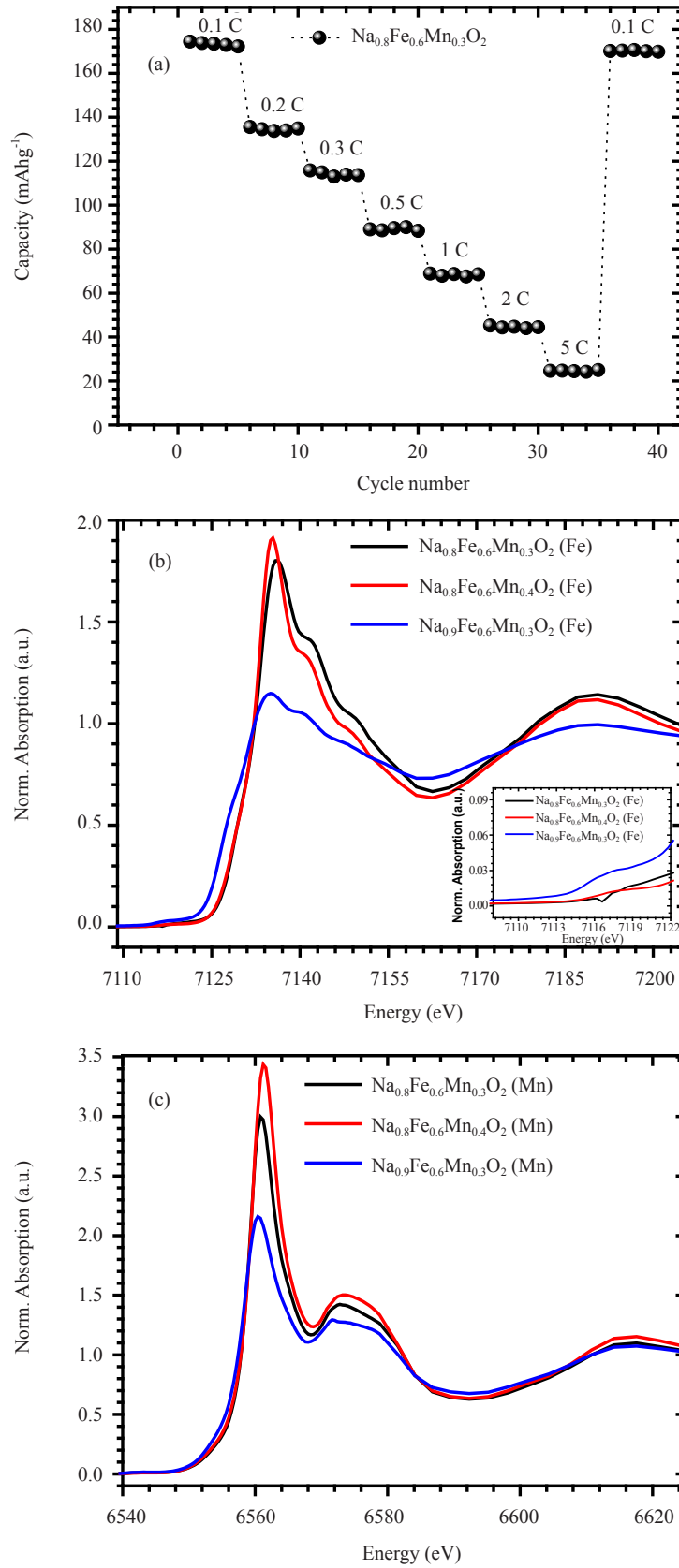
Figure 5. (a) Specific C-rate discharge capacity of best sample containing $Na_{0.8}Fe_{0.6}Mn_{0.3}O_2$ at various rates. (b, c) shows XANE spectra analysis containing Fe and Mn metals with $Na_{0.8}Fe_{0.6}Mn_{0.3}O_2$, $Na_{0.8}Fe_{0.6}Mn_{0.4}O_2$, $Na_{0.9}Fe_{0.6}Mn_{0.3}O_2$ combinations, respectively

Figure 5 shows the electrochemical behavior of our best synthesized sample with composition $Na_{0.8}Fe_{0.6}Mn_{0.3}O_2$ upon C-rate tests at current rates of 0.1 C, 0.2 C, 0.5 C, 1 C, and 5 C and ending with 0.1 C within the potential range 2.0 V to 3.8 V and it shows the superior performance with the specific charge capacity (0.1 C = 179 mAhg^{-1}, 0.2 C = 140 mAhg^{-1}, 0.3 C = 128 mAhg^{-1}, 0.5 C = 85 mAhg^{-1}, 1 C = 72 mAhg^{-1}, 5 C = 28 mAhg^{-1}). The capacity fading of phase pure layered oxides upon cycling results from the occurring phase transitions, which are accompanied by large volume changes. In fact, the c-axis parameter of layered Na-based oxides is known to change dramatically upon sodium (de-) intercalation and phase transitions with the latter usually observed at higher potentials. Furthermore, the X-ray Analysis Near Edge (XANE) spectra were analyzed at the Fe-K edge structures to ascertain the oxidation states, local symmetry and electronic structure of Fe and Mn constituents in samples $Na_{0.8}Fe_{0.6}Mn_{0.4}O_2$, $Na_{0.8}Fe_{0.6}Mn_{0.3}O_2$, $Na_{0.9}Fe_{0.6}Mn_{0.3}O_2$, respectively. It is known that positions of absorption pre-edge (1s-3d) transition and edge (1s-4p) resonance are sensitive to Fe oxidation states. The pre-edge appears at ~7115 eV for Fe^{3+} species responsible for site symmetry where the lower intensity of these peaks is highly responsible for high symmetry structure as can be seen in the inset graph. Moreover, a prominent peak also denotes the structure is distorted octahedral or tetrahedral but in our case peak is very low which indicates a clear octahedral system. The absorption pre-edge and edge found for all samples at 7114.5 eV and 7125 eV, hints at Fe^{3+} species [33]. However, additional small peaks at 7146 eV have been observed for ferrihydrite (Fh-FeOOH), where Fe(III) cations are coordinated with O atoms and terminal OH species in both tetrahedral and octahedral geometries that shows samples even on short exposure at measuring condition absorbs moisture although the samples for electrochemical analysis kept in glove box conditions to avoid moisture absorption. The absorption edge position was agreed with that of iron and the edge energy of $Na_{0.8}Fe_{0.6}Mn_{0.3}O_2$, $Na_{0.8}Fe_{0.6}Mn_{0.4}O_2$, $Na_{0.9}Fe_{0.6}Mn_{0.3}O_2$ were 7140, 7139 and 7135 eV, respectively. The decrease in energy shift of 5 eV in $Na_{0.9}Fe_{0.6}Mn_{0.3}O_2$ indicates a decrease in the oxidation state of Fe ions. The whole spectra show two isosbestic points at 7130 eV and 7175 eV indicative of Fe^{3+} phases. The inset shows that the enlarged pre-edge features present a less intense peak indicating octahedral structure and sample $Na_{0.9}Fe_{0.6}Mn_{0.3}O_2$ shows lower energy shifts of possible some Fe^{2+} feature. In Figure 5(b), the K-edge of Mn shifts to higher energies with increment in intensities with Mn content ($Na_{0.8}Fe_{0.6}Mn_{0.4}O_2$) than other samples where Mn content is less. It is worthy to observe that the pre-edge peak intensity in Mn (6560 eV) is more affected by slight (0.1 Na) increment confirms non-local dipole characteristics of high energy peak describing intensity correlates well with 4p-O-3d hybridization.

4. Conclusions

In this work, we investigated transition metals Fe to Mn constituent in the sodium magnate layered cathode for high performing sodium-ion batteries with compositions of $Na_{0.8}Fe_{0.4}Mn_{0.5}O_2$, $Na_{0.8}Fe_{0.5}Mn_{0.4}O_2$, $Na_{0.8}Fe_{0.6}Mn_{0.3}O_2$, $Na_{0.8}Fe_{0.6}Mn_{0.4}O_2$, $Na_{0.8}Fe_{0.7}Mn_{0.4}O_2$, $Na_{0.9}Fe_{0.6}Mn_{0.3}O_2$, and observed best with the $Na_{0.8}Fe_{0.6}Mn_{0.3}O_2$ combination with O3-R3m space group. The charge-discharge capacities in the range of 2.0-3.8 V at 0.1 C show higher performance of the first and second charge capacity 115 and 180 mAhg^{-1} and discharge capacity of 184 and 181 mAhg^{-1}, respectively. The suitability of this combination lies in its biphasic electrochemical behavior demonstrating reduced Jahn-Teller effect with Fe^{3+} excess, substituting (Fe^{3+}) effect of vacancy ordering of Mn and enhancing crystallinity of 41.5 ° in XRD peaks. The CV results show a higher anodic/cathode peak (1.73 V/2.2 V) due to Fe substitution while Rielveldt refinement shows pure O-3 crystal structure in the best sample but $Na_{0.8}Fe_{0.6}Mn_{0.4}O_2$, $Na_{0.9}Fe_{0.6}Mn_{0.3}O_2$ shows P-type (Cmca space group) behavior with 30.8% and 32.8%, respectively. The reported result clearly indicates that different Fe and Mn ratios substantially affect the electrochemical behavior in O3-type layered cathodes.

Conflict of interest

The authors declare that there are no conflicts of interest.

References

[1] Ambrose H, Kendall A. Understanding the future of lithium: Part 1, resource model. *Journal of Industrial Ecology*. 2020; 24(1): 80-89. Available from: doi: 10.1111/jiec.12949.

[2] Hong SY, Kim Y, Park Y, Choi A, Choi NS, Lee KT. Charge carriers in rechargeable batteries: Na ions vs. Li ions. *Energy & Environmental Science*. 2013; 6: 2067-2081. Available from: doi: 10.1039/C3EE40811F.

[3] Deng J, Luo WB, Chou SL, Liu HK, Dou SX. Sodium-ion batteries: from academic research to practical commercialization. *Advanced Energy Materials*. 2018; 8(4): 1701428. Available from: doi: 10.1002/aenm.201701428.

[4] Bin D, Wang F, Tamirat AG, Suo L, Wang Y, Wang C, et al. Progress in aqueous rechargeable sodium-ion batteries. *Advanced Energy Materials*. 2018; 8(17): 1703008. Available from: doi: 10.1002/aenm.201703008.

[5] Chen M, Zhang Y, Xing G, Tang Y. Building high power density of sodium-ion batteries: importance of multidimensional diffusion pathways in cathode materials. *Frontiers in Chemistry*. 2020; 8: 152. Available from: doi: 10.3389/fchem.2020.00152.

[6] Liu Q, Hu Z, Chen M, Zou C, Jin H, Wang S, et al. The cathode choice for commercialization of sodium-ion batteries: layered transition metal oxides versus Prussian blue analogs. *Advanced Functional Materials*. 2020; 30(14): 1909530. Available from: doi: 10.1002/adfm.201909530.

[7] Palomares V, Serras P, Villaluenga I, Hueso KB, Carretero-Gonzalez J, Rojo T. Na-ion batteries, recent advances and present challenges to become low cost energy storage systems. *Energy & Environmental Science*. 2012; 5: 5884-5901. Available from: doi: 10.1039/C2EE02781J.

[8] Kim SW, Seo DH, Ma X, Ceder G, Kang K. Electrode materials for rechargeable sodium-Ion batteries: Potential alternatives to current lithium-ion batteries. *Advanced Energy Materials*. 2012; 2(7): 710-721. Available from: doi: 10.1002/aenm.201200026.

[9] Delmas C, Braconnier JJ, Fouassier C, Hagenmuller P. Electrochemical intercalation of sodium in Na_xCoO_2 bronzes. *Solid State Ionics*. 1981; 3-4: 165-169. Available from: doi: 10.1016/0167-2738(81)90076-X.

[10] Abraham KM. Intercalation positive electrodes for rechargeable sodium Cells. *Solid State Ionics*. 1982; 7(3): 199-212. Available from: doi: 10.1016/0167-2738(82)90051-0.

[11] Nagaura N, Tozawa K. Lithium ion rechargeable battery. *Progress in Batteries and Solar Cells*. 1990; 9: 209-213.

[12] Emery N, Baddour-Hadjeon R, Batyrbekuly D, Laik B, Bekenov Z, Pereira-Ramos JP. γ-$Na_{0.96}V_2O_5$: A new competitive cathode material for sodium ion battery synthesized by soft chemistry route. *Chemistry of Materials*. 2018; 30(15): 5305-5314. Available from: doi: 10.1021/acs.chemmater.8b02066.

[13] Han MH, Gonzalo E, Singh G, Rojo T. A comprehensive review of sodium layered oxides: Powerful cathodes for Na-ion batteries. *Energy & Environmental Science*. 2015; 8: 81-102. Available from: doi: 10.1039/C4EE03192J.

[14] Dai Z, Mani U, Tan HT, Yan Q. Advanced cathode materials for sodium ion batteries: What determine our choices? *Small Methods*. 2017; 1(5): 1700098. Available from: doi: 10.1002/smtd.201700098.

[15] Delmas C, Fouassier C, Hagenmuller P. Structural classification and properties of layered oxides. *Physica B + C*. 1980; 99(1-4): 81-85. Available from: doi: 10.1016/0378-4363(80)90214-4.

[16] Ma X, Chen H, Ceder G. Electrochemical properties of monoclinic $NaMnO_2$. *Journal of The Electrochemical Society*. 2011; 158: A1307-A1312. Available from: doi: 10.1149/2.035112jes.

[17] Yabuuchi N, Kajiyama M, Iwatate J, Nishikawa H, Hitomi S, Okuyama R, et al. P2-type $Na_x[Fe_{1/2}Mn_{1/2}]O_2$ made from earth-abundant elements for rechargeable Na batteries. *Nature Materials*. 2012; 11: 512-517.

[18] Komaba S, Takei C, Nakayama T, Ogata A, Yabuuchi N. Electrochemical intercalation activity of layered $NaCrO_2$ vs. $LiCrO_2$. *Electrochemistry Communications*. 2010; 12: 355-358. Available from: doi: 10.1016/j.elecom.2009.12.033.

[19] Wang PF, You Y, Yin YX, Guo YG. Layered oxide cathodes for sodium-ion batteries: phase transition, air stability, and performance. *Advanced Energy Materials*. 2018; 8(8): 1701912. Available from: doi: 10.1002/aenm.201701912.

[20] Hasa I, Buchholz D, Passerini S, Scrosati B. High performance $Na_{0.5}[Ni_{0.23}Fe_{0.13}Mn_{0.63}]O_2$ cathode for sodium-ion batteries. *Advanced Energy Materials*. 2014; 4(15): 1400083. Available from: doi: 10.1002/aenm.201400083.

[21] Komaba S, Yabuuchi N, Nakayama T, Ogata A, Ishikawa T, Nakai I. Study on the reversible electrode reaction of $Na_{1-x}Ni_{0.5}Mn_{0.5}O_2$ for a rechargeable sodium-ion battery. *Inorganic Chemistry*. 2012; 51: 6211-6220. Available from: doi: 10.1021/ic300357d.

[22] Wang H, Yang B, Liao XZ, Xu J, Yang D, Yang D, et al. Electrochemical properties of P2-$Na_{2/3}[Ni_{1/3}Mn_{2/3}]O_2$ cathode material for sodium ion batteries when cycled in different voltage ranges. *Electrochimica Acta*. 2013; 113:

200-204. Available from: doi: 10.1016/j.electacta.2013.09.098.

[23] Parant JP, Olazcuaga R, Devalette, Fouassier C, Hagenmuller P. Sur quelques nouvelles phases de formule Na_xMnO_2 (x ≤ 1) [On some new formula phases Na_xMnO_2 (x ≤ 1)]. *Journal of Solid State Chemistry*. 1971; 3: 1-11. Available from: doi: 10.1016/0022-4596(71)90001-6.

[24] Yuan Z, Xuehang W, Wenwei W, Kaitu W. Synthesis and electrochemical performance of $Na_{0.7}Fe_{0.7}Mn_{0.3}O_2$ as cathode material for Na-ion battery. *Ceramics International*. 2014; 40: 13679-13682. Available from: doi: 10.1016/j.ceramint.2014.04.126.

[25] Zhao J, Xu J, Lee DH, Dimov N, Meng YS, Okada S. Electrochemical and thermal properties of P2-type $Na_{2/3}Fe_{1/3}Mn_{2/3}O_2$ for Na-ion batteries. *Journal of Power Sources*. 2014; 264: 235-239. Available from: doi: 10.1016/j.jpowsour.2014.04.048.

[26] Noh HJ, Youn S, Yoon CS, Sun YK. Comparison of the structural and electrochemical properties of layered $Li[Ni_xCo_yMn_z]O_2$ (x ¼ 1/3, 0.5, 0.6, 0.7, 0.8 and 0.85) cathode material for lithium-ion batteries. *Journal of Power Sources*. 2013; 233: 121-130. Available from: doi: 10.1016/j.jpowsour.2013.01.063.

[27] Khan MA, Han D, Lee G, Kim YI, Kang YM. P2/O3 Phase-integrated $Na_{0.7}MnO_2$ cathode materials for sodium ion rechargeable batteries. *Journal of Alloys and Compounds*. 2019; 771: 987-993. Available from: doi: 10.1016/j.jallcom.2018.09.033.

[28] Yabuuchi N, Yano M, Yoshida H, Kuze S, Komaba S. Synthesis and electrode performance of O3-type $NaFeO_2$-$NaNi_{1/2}Mn_{1/2}O_2$ solid solution for rechargeable sodium batteries. *Journal of The Electrochemical Society*. 2013; 160(5): A3131-A3137. Available from: doi: 10.1149/2.018305jes/meta.

[29] Anang DA, Bhange DS, Ali B, Nam KW. New O3 type layer-structured $Na_{0.80}[Fe_{0.40}Co_{0.40}Ti_{0.20}]O_2$ cathode materials for rechargeable sodium ion batteries. *Materials*. 2021; 14(9): 2363. Available from: doi: 10.3390/ma14092363.

[30] Keller M, Buchholz D, Passerini S. Layered Na-ion cathodes with outstanding performance resulting from the synergetic effect of mixed P- and O-type phases. *Advanced Energy Materials*. 2016; 6(3): 1501555. Available from: doi: 10.1002/aenm.201501555.

[31] Yuan D, Hu X, Qian J, Pei F, Wu F, Mao R, et al. P2-type $Na_{0.67}Mn_{0.65}Fe_{0.2}Ni_{0.15}O_2$ cathode material with high-capacity for sodium-ion battery. *Electrochimica Acta*. 2014; 116: 300-305. Available from: doi: 10.1016/j.electacta.2013.10.211.

[32] Thorne JS, Dunlap RA, Obrovac MN. Structure and electrochemistry of $Na_xFe_xMn_{1-x}O_2$ (1.0 ≤ x ≤ 0.5) for Na-ion battery positive electrodes. *Journal of The Electrochemical Society*. 2012; 160: A361-A367. Available from: doi: 10.1149/2.058302jes.

[33] Carta D, Casula MF, Corrias A, Falqui A, Navarra G, Pinna G. Structural and magnetic characterization of synthetic ferrihydrite nanoparticles. *Materials Chemistry and Physics*. 2009; 113: 349-355. Available from: doi: 10.1016/j.matchemphys.2008.07.122.